Journal of Medicinal Chemistry Article

J. Med. Chem. **2009,** *52,* 7753–7764 **7753**
DOI: 10.1021/jm900731j

Amide Linkage Isomerism As an Activity Switch for Organometallic Osmium and Ruthenium Anticancer Complexes

Sabine H. van Rijt,[†] Andrew J. Hebden,[‡] Thakshila Amaresekera,[‡] Robert J. Deeth,[†] Guy J. Clarkson,[†] Simon Parsons,[§] Patrick C. McGowan,*[,‡] and Peter J. Sadler*[,†]

[†]*Department of Chemistry, University of Warwick, Gibbet Hill Road, Coventry CV4 7AL, U.K.,* [‡]*School of Chemistry, University of Leeds, Leeds LS2 9JT, U.K., and* [§]*School of Chemistry, University of Edinburgh, West Mains Road, Edinburgh EH9 3JJ, U.K.*

Received May 28, 2009

We show that the binding mode adopted by picolinamide derivatives in organometallic Os^{II} and Ru^{II} half-sandwich complexes can lead to contrasting cancer cell cytotoxicity. *N*-Phenyl picolinamide derivatives (XY) in Os^{II} (**1**, **3**−**5**, **7**, **9**) and Ru^{II} (**2**, **6**, **8**, **10**) complexes $[(\eta^6\text{-arene})(Os/Ru)(XY)Cl]^{n+}$, where arene = *p*-cymene (**1**−**8**, **10**) or biphenyl (**9**), can act as *N*,*N*- or *N*,*O*-donors. Electron-withdrawing substituents on the phenyl ring resulted in *N*,*N*-coordination and electron-donating substituents in *N*,*O*-coordination. Dynamic interconversion between *N*,*O* and *N*,*N* configurations can occur in solution and is time- and temperature- (irreversible) as well as pH-dependent (reversible). The neutral *N*,*N*-coordinated compounds (**1**−**5** and **9**) hydrolyzed rapidly ($t_{1/2} \leq$ min), exhibited significant (32−70%) and rapid binding to guanine, but no binding to adenine. The *N*,*N*-coordinated compounds **1**, **3**, **4**, and **9** exhibited significant activity against colon, ovarian, and cisplatin-resistant ovarian human cancer cell lines (**3** ≫ **4** > **1** > **9**). In contrast, *N*,*O*-coordinated complexes **7** and **8** hydrolyzed slowly, did not bind to guanine or adenine, and were nontoxic.

Introduction

There is an intriguing interplay between oxygen and nitrogen binding of amides to metal ions in coordination complexes.[1] Amide groups are usually planar, with the C−N bond possessing some 40% double-bond character. Metal ions tend to interact only weakly with the carbonyl oxygen of a neutral amide group, but this is strengthened if there is a nearby anchoring group so that a chelate ring can form. However, this interaction remains weak. The deprotonated amide nitrogen is a much stronger metal binding site (ca. 10^{16} more basic than the neutral amide); a site which becomes more favorable at higher pH, although it has to compete with metal ion hydrolysis. Binding to a deprotonated amide N is also strengthened when there is an anchoring group that allows a 5- or 6-membered chelate ring to form. There are only a few reported examples of pairs of linkage isomers; these include N- and O- bonded monodentate amide adducts of $(NH_3)_5Co^{II}$,[2,3] $dienPt^{II}$,[4−6] and $(NH_3)_4Ru^{III}$,[7,8] however these could not be interconverted.

Metal complexes with picolinamide ligands have previously received attention because of their relevance to peptide chemistry.[9−11] These ligands are known to bind to metal ions either as neutral *N*,*O*-donors, or as monoanionic *N*,*N*-donors via loss of the amide proton. For example, complexes with the first row transition metals Fe^{II}, Co^{II}, Ni^{II} Cu^{II}, and Zn^{II} mostly involve *N*,*O*-donation.[12,13] The anionic *N*,*N*-donor form of the picolinamide ligand is able to stabilize first row metal ions in high (≥+3) oxidation states due to its strong σ-donor capability,[14] and also some *N*,*N* coordination complexes of Ru^{II} are known.[15] In the present work, we have investigated the influence on cancer cell cytoxicity of nitrogen, nitrogen (*N*,*N*) versus nitrogen, oxygen (*N*,*O*) coordination of picolinamide derivatives containing an anchoring pyridyl ring in Os^{II} and Ru^{II} arene complexes.

A number of ruthenium compounds has previously been shown to display promising anticancer activity,[16] and two Ru^{III} complexes have entered clinical trials, *trans*-$[RuCl_4(DMSO^a)(Im)]$ImH (NAMI-A, where Im = imidazole) and *trans*-$[RuCl_4(Ind)_2]$IndH (KP1019, where Ind = indazole). It is believed that the activity of the Ru^{III} compounds is dependent on the in vivo reduction to the more reactive Ru^{II} species.[17] This has led to increased interest into the anticancer potential of Ru^{II} compounds, and Ru^{II} "half-sandwich" arene complexes, for example, exhibit both in vitro and in vivo activity.[18] Also, our recent work has shown that analogues containing the heavier congener osmium can also be potently cytotoxic toward cancer cells with activity that is comparable to the clinical drugs carboplatin and cisplatin.[19,20]

We show here that the binding mode exhibited by picolinamide derivatives in Os^{II} and Ru^{II} arene complexes can have a major effect on the cancer cell cytotoxicity of these complexes and attempt to relate this not only to their solid-state structures but also to their hydrolysis rates, to the acidity of the resulting aqua adducts, and nucleobase binding. This

*To whom correspondence should be addressed. For P.J.S.: phone, (+44) 024 7652 3818; fax, (+44) 024 76523819; E-mail, p.j.sadler@warwick.ac.uk. For P.C.M.: phone, (+44) 0113 3436404; fax, (+44) 0113 343 6565; E-mail: P.C.McGowan@leeds.ac.uk.

[a] Abbreviations: bip, biphenyl; *p*-cym, *para*- cymene; cisplatin, *cis*-diamminedichloridoplatinum(II); RPMI, Roswell Park Memorial Institute; DMSO, dimethylsulfoxide; IC_{50}, concentration inhibiting cell growth by 50%; SRB, sulforhodamine B; 9EtG; 9-ethyl guanine; 9EtA, 9-ethyl adenine.

© 2009 American Chemical Society

Published on Web 09/30/2009

Chart 1. Osmium and Ruthenium Arene Complexes Studied in This Work and the Structures of 9-Ethyl Guanine and 9-Ethyl Adenine

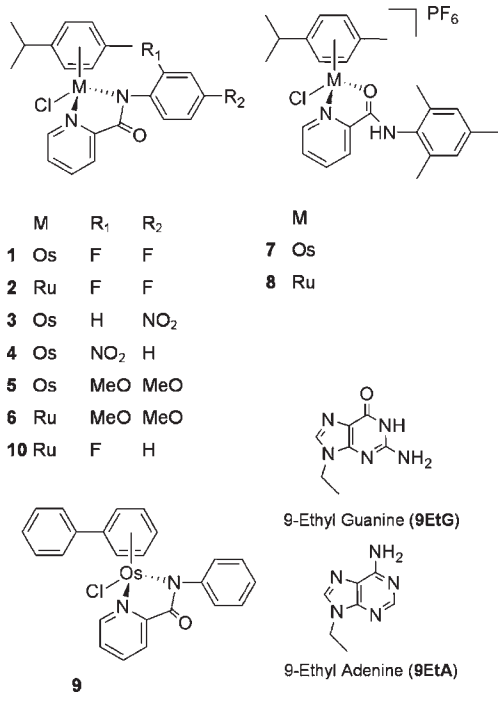

study demonstrates that the substituents on the ligands in this type of complex can have marked effects on the configuration adopted by the complexes and their reactivity and might provide a route to "fine-tune" and switch their biological activity.

Results

Synthesis and Characterization. Novel half-sandwich osmium(II) and ruthenium(II) arene complexes with *N*-Ph-picolinamide derivatives (Chart 1) were synthesized from the chlorido-bridged dimers, $[(\eta^6\text{-}p\text{-cym})MCl_2]_2$ (where M is Os or Ru) and $[(\eta^6\text{-bip})OsCl_2]_2$. Osmium complexes containing electron-withdrawing substituents on the phenyl ring could be isolated as their neutral *N*,*N*-coordinated forms (**1**, **3**, **4**, and **9** and Ru^{II} complex **2**, Chart 1). The isolation of *N*,*O*-coordinated picolinamide complexes was successful only when the Ph-picolinamide ligand contained electron-donating methyl groups for both the osmium (**7**) and ruthenium compounds (**8**) (Chart 1). This *N*,*O*-binding mode was confirmed by their X-ray crystal structures. Both *N*,*N*- and *N*,*O*- coordination modes were observed for compound **5** when no PF_6^- anion was added. However, after addition of PF_6^-, *N*,*N*-coordination was observed by ^{1}H NMR. This can be accounted for the binding of a proton as a bridge between the carboxamide oxygens of two molecules of the complex forming a cationic dimeric species, so explaining the role of the counteranion PF_6^-. Such a dimeric structure was also found in the crystal structure of the ruthenium analogue **6** (Figure 1C) and is described below.

X-ray crystal structures were obtained for compounds $[(\eta^6\text{-}p\text{-cym})Os(N\text{-}2,4\text{-difluoro-Ph-picolinamide})Cl]$ (**1**), $[(\eta^6\text{-}p\text{-cym})Ru(N\text{-}2,4\text{-difluoro-Ph-picolinamide})Cl]$ (**2**), $[(\eta^6\text{-}p\text{-cym})Os(N\text{-}4\text{-nitro-Ph-picolinamide})Cl]\cdot MeOD$ (**3**·MeOD), $[(\eta^6\text{-}p\text{-cym})Ru(N\text{-}2,4\text{-dimethoxide-Ph-picolinamide})Cl]_2HPF_6$ (**[6-H-6]PF$_6$**), $[(\eta^6\text{-}p\text{-cym})Os(N\text{-}2,4,6\text{-trimethyl-Ph-picolinamide})Cl]PF_6\cdot CH_2Cl_2$ (**7**·CH_2Cl_2), and $[(\eta^6\text{-}p\text{-cym})Ru(N\text{-}2,4,6\text{-trimethyl-Ph-picolinamide})Cl]PF_6$ (**8**·$CHCl_3$), Figure 1A−D and Figure S1A,B (Supporting Information, SI). All complexes adopt the familiar pseudo-octahedral "three-legged piano stool" geometry. Ruthenium and osmium are π-bonded to the *p*-cymene ring ("the seat") and σ-bonded to a chloride and to a chelated *N*-Ph-picolinamide ligand. The latter is bound through both nitrogens (pyridyl and amidinato nitrogen, *N*,*N*-coordination) in **1**, **2**, **3**, and **6** and through the pyridyl nitrogen and carboxamide oxygen (*N*,*O*-coordination) in **7** and **8**. These atoms, together with Cl, constitute the three legs of the piano stool. Crystallographic data, selected bond lengths, and angles are given in Tables S1 and S2 of the SI.

Intermolecular H-bonding between C26−H···F17 (2.479 Å) and intramolecular H-bonding between C15−H···F14 (2.547 Å) and between C24−H···O8 (2.212 Å) is observed in the crystal structure of **1** (Figure S2A, SI). In addition, there is an offset π-stacking interaction between the *p*-cymene arene and the substituted phenyl of adjacent molecules with a centroid-to-centroid distance of 3.71 Å (plane tilt of 14°). The molecular structure (Figure S1A, SI) and crystal cell data (Table S1, SI) obtained for **2** are similar to those of Os congener **1**, although the M-Cl bond is significantly shorter (i.e., M-Cl: 2.4434(14) Å for **1**, 2.4126(4) Å for **2**). The crystal structure of **3** contains a molecule of methanol in the asymmetric unit. There is an offset weak π-stacking interaction between two pyridyls of adjacent molecules with a centroid-to-centroid distance of 4.06 Å (Figure 2SB, SI). In addition, there is H-bonding between the amidinato carboxylate and methanol solvent molecule (1.93 Å, Figure S2B, SI). Remarkably, the bond distances of *N*,*N*-coordinated osmium complex **3** are more comparable to *N*,*N*-coordinated ruthenium complex **2** than to *N*,*N*-coordinated osmium complex **1**, with in particular the M-Cl bond length (i.e., M-Cl: 2.4434(14) Å for **1**, 2.4050(6) Å for **2**, and 2.4126(4) for **3**·MeOD, Table S2, SI).

The crystal structure of the dimethoxyphenylpicolinamide ruthenium complex **6** contains half a PF_6^- anion in the asymmetric unit. Inspection of the remainder of the structure indicated a short intramolecular distance of 2.425 Å between the oxygen atoms O7 in neighboring symmetry-related molecules. This suggests that there is an O−H−O bond linking two neighboring ruthenium fragments that would provide appropriate charge balance for the anion (Figure 1C). However, this hypothetical H atom could not be located in the Fourier map. For the related complex, $[(\eta^6\text{-}p\text{-cym})Ru(N\text{-}2\text{-fluoro-Ph-picolinamide})Cl]$ (**10**), the X-ray structure of the dimer **[10-H-10]PF$_6$** (Figure S3, Table S3, SI) also has the O−H−O motif and a PF_6^- anion and the H atom in the O−H−O motif could be located in the Fourier map, resulting in a linear O−H−O bond. Accordingly, for **6**, the H atom in the O−H−O bond was placed in a fixed calculated position such that the bond O−H−O was linear (Figure 1C).

The X-ray structures of **7** and **8** revealed *N*,*O*-coordination for the picolinamide ligand. The cationic Os compound **7**, where PF_6^- acts as a counterion, crystallizes with one solvent molecule of dichloromethane. The phenyl ring of the *N*-Ph-picolinamide ligand is almost perpendicular to the pyridine ring with a plane angle of 82.19° (72.64° for **1**, Figure 1D). The Os−Cl bond distance in compound **7**·CH_2Cl_2 is short compared to compound **1** (i.e., Os−Cl 2.3878(10) Å for **7**·CH_2Cl_2, 2.4434(14) Å for **1**). A 1:1 enantiomeric ratio of $S_{Os/Ru}$:$R_{Os/Ru}$ was observed in the crystal lattices of all compounds. The same ratio was observed for **7** in solution by ^{1}H NMR ($CDCl_3$, 298 K) on

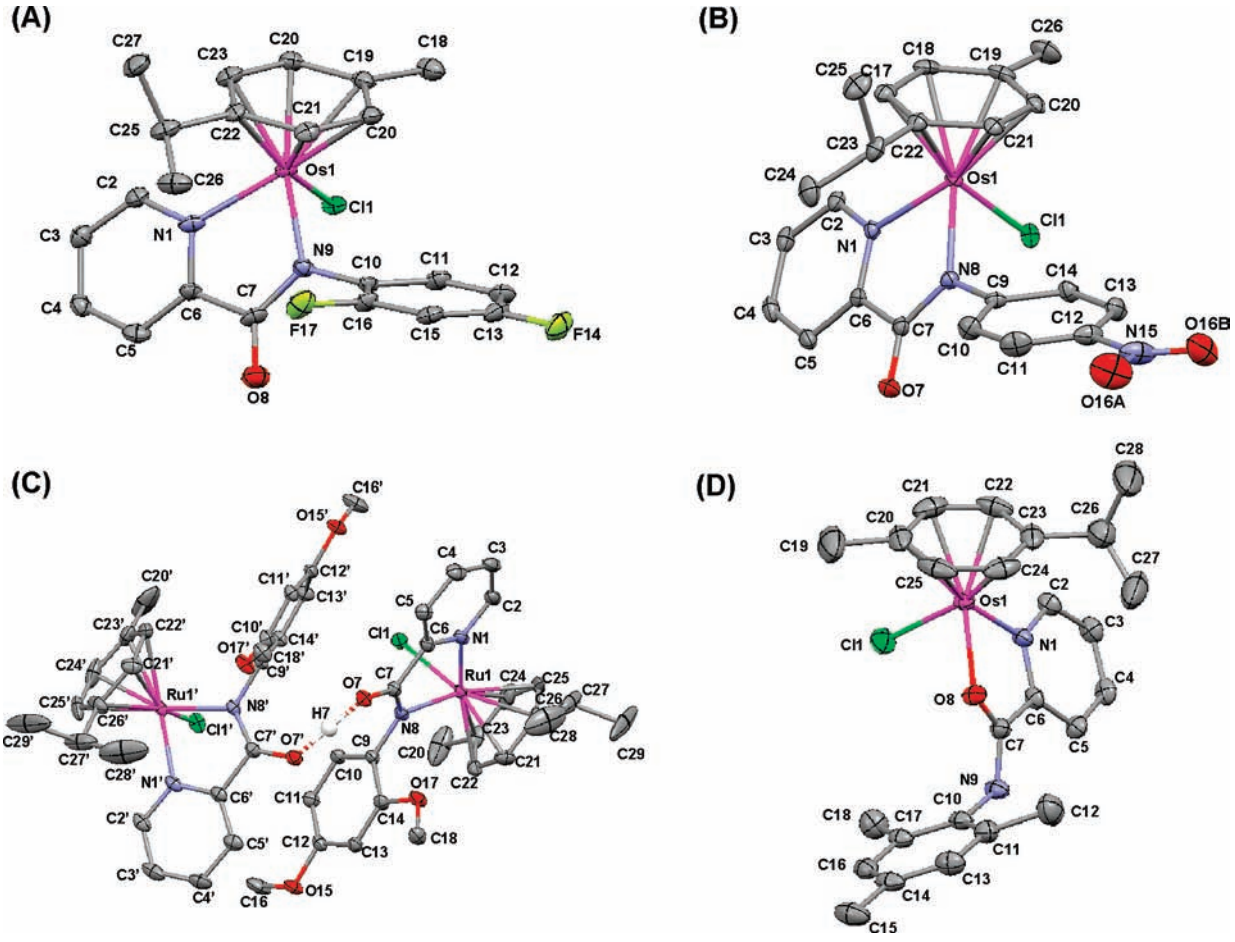

Figure 1. X-ray structures and atom numbering schemes for complexes (A) [(η^6-*p*-cym)Os(*N*-2,4-difluoro-Ph-picolinamide)Cl] (**1**), (B) [(η^6-*p*-cym)Os(*N*-4-nitro-Ph-picolinamide)Cl]·MeOD (**3**·MeOD), (C) [(η^6-*p*-cym)Ru(*N*-2,4-dimethoxide-Ph-picolinamide)Cl]$_2$HPF$_6$ (**[6-H-6]PF$_6$**), and (D) [(η^6-*p*-cym)Os(*N*-2,4,6-trimethyl-Ph-picolinamide)Cl]PF$_6$·CH$_2$Cl$_2$ (**7**·CH$_2$Cl$_2$). Hydrogen atoms, except the bridging H in **6** (C), solvents, and counterions are omitted for clarity.

addition of the chiral anionic shift reagent TRISPHAT (Figure S4, SI). No attempt was made to separate the enantiomers. The cationic ruthenium compound **8**, with PF_6^- as the counterion, crystallizes with one solvent molecule of chloroform (Figure S1B, SI). The methyl and isopropyl groups on the *p*-cymene ring are disordered over two positions with occupancy of 0.5. The Ru−Cl and Ru−O bond lengths of compound **8** are very similar to that of the osmium analogue **7** (i.e., M-Cl: 2.3853(11) Å for **8**·CHCl$_3$, 2.3878(10) Å for **7**·CH$_2$Cl$_2$: and M-O: 2.118(3) for **8**·CHCl$_3$, 2.117(2) for **7**·CH$_2$Cl$_2$). The Ru−Cl bond of **8** is shorter than for Ru compounds **2** and **[6-H-6]PF$_6$** (i.e., Ru−Cl 2.3853(11) Å for **8**·CHCl$_3$, 2.4050(6) Å for **2**, and 2.4114(11) Å for **[6-H-6]PF$_6$**)

Kinetic NMR studies. During the preparation of compounds **1**−**4** and **9**, an equilibrium between the two configurations was often observed by ^{1}H NMR (in MeOD-d_4 and DMSO-d_6). However, upon longer reaction times and recrystallization from dichloromethane, Os complexes **1**, **3**, **4**, and **9** and Ru complex **2** could be isolated as their neutral *N*,*N*-coordinated forms (Chart 1). To investigate the nature of the equilibrium between the *N*,*O*- and *N*,*N*-coordination observed for products isolated from the syntheses of complexes **1**−**4** and **9**, a 50:50 mixture of **3** (obtained as a sticky solid) was studied as a function of temperature, time, and pH. ^{1}H NMR spectra of the *N*,*O*- and *N*,*N*-coordinated mixture of **3** (50:50) in MeOD-d_4 were recorded over the temperature range 173−323 K. From 173 K up to 283 K, the ratio between *N*,*O*- and *N*,*N*-coordination remained at about 50:50. However, above 283 K, the *N*,*N*-coordinated linkage isomer of **3** was favored, and by 323 K, a full conversion to the *N*,*N*-coordinated compound was observed (Figure S5, SI). This process was independent of the deuterated solvent (D$_2$O, DMSO-d_6, MeOD-d_4, CDCl$_3$ at 298 K) and was irreversible after a 48 h period at ambient temperature after recording the ^{1}H NMR spectrum at 298 K. Also, it was found to be possible to obtain a higher ratio of *N*,*O*-coordination versus *N*,*N*-coordination by synthesizing **3** at lower temperatures. This typically resulted in the formation of only the *N*,*N*-coordinated linkage isomer after 3-day storage of the mixture in solution at ambient temperature.

To investigate the effect of pH on the 50:50 equilibrium mixture of the configurational isomers of **3**, ^{1}H NMR spectra of **3** in D$_2$O were recorded over the pH* (pH meter reading for a D$_2$O solution) range of 2−9. When the pH was increased from 2 to 9, a full conversion from *N*,*O*- to *N*,*N*-coordination was observed (Figure S6, SI). At an acidic pH* of 2, only the *N*,*O*-isomer of **3** was observed, while at pH* 8.5, only the *N*,*N*-analogue of **3** was present. This process was found to be reversible. The onset of conversion of *N*,*O*- into *N*,*N*-coordination appeared to occur when the pH* was raised above ca. pH* 7.

Hydrolysis Data. The rate of hydrolysis of compounds **1**−**5** and **7**−**9** in a 5% MeOD-d_4/95% D$_2$O mixture was monitored by ^{1}H NMR at 288 K by observation of new

Table 1. Hydrolysis Data for Complexes **1**−**5** and **7**−**9** at 288 K Determined by ^{1}H NMR

compd	k, h^{-1}	$t_{1/2}$, h
1	≥5.9	≤0.12
2	≥5.9	≤0.12
3	≥5.9	≤0.12
4	≥5.9	≤0.12
5	≥5.9	≤0.12
7	0.16 ± 0.03	4.33 ± 0.68
8	1.63 ± 0.05	0.42 ± 0.02
9	≥5.9	≤0.12

Table 2. pK_a* Values for the Deprotonation of the Coordinated D_2O in Aqua Adducts of Complexes **1**, **7** and of the Amide Proton in Compound **7**

compd	pK_a* aqua adduct	pK_a* NH
1	7.33	
7	7.08	7.62

peaks over time due to aqua adduct formation. To ensure that the hydrolysis rates were determined for the *N*,*N*-coordinated isomers (e.g., for complex **3**, the *N*,*O*-isomer is formed reversibly at low pH), we determined the hydrolysis rates at pH ∼ 7. All complexes, except *N*,*O*-coordinated complexes **7** and **8**, hydrolyzed rapidly with half-lives too short to measure by ^{1}H NMR ($t_{1/2}$ ≤ 10 min; time needed to record the first ^{1}H NMR spectrum). The percentage of aqua peak formation for **7** and **8** was plotted against time and fitted to pseudo-first-order kinetics to give half-lives of 4.33 and 0.42 h, respectively (Table 1).

pK_a* Determination. Changes in the ^{1}H NMR chemical shifts for the protons of the coordinated *p*-cymene ring in compounds **1** and **7**, present in equilibrium aqueous solutions of **1** or **7** containing their aqua adducts as the major species, were followed over the pH* range 2−9 (Figure S7, SI). When the pH* values of the solutions were increased, the major set of NMR peaks assigned to the aqua adducts of **1** and **7** gradually shifted to higher field in the spectrum. For compound **7**, the two sets of peaks, assigned to the aqua and chlorido adducts, shifted to high field as a result of amide proton loss with increasing pH*. The chemical shift was plotted against pH*, and the resulting pH* titration curves were fitted to the modified Henderson−Hasselbalch equation.[21,22] This gave rise to similar pK_a* values for the coordinated water of 7.3 for **1** and 7.1 for **7**. The amide proton in compound **7** gave a pK_a* value of 7.6 (Table 2).

Cancer Cell Cytotoxicity. The cytotoxicity of the complexes toward colon HCT116, ovarian A2780, and ovarian cisplatin resistant A2780cis cancer cell lines was investigated. Complexes **7**, **8**, and **5** were found to be nontoxic in all three cell lines up to the highest test concentration of 50 μM. Their IC_{50} values (concentration at which 50% of the cell growth is inhibited) are therefore likely to be >100 μM, and the compounds can therefore be described as inactive. However, promising activity was observed for the neutral *N*,*N*-coordinated compounds **1**, **3**, **4**, and **9** (Table 3, Figure S8, SI). A trend in cytotoxic activity is observed in all three cell lines, following the order of **3** ≫ **4** > **1** > **9** (Chart 1). Complex **3**, [(η^6-*p*-cym)Os(*N*-4-nitro-Ph-picolinamide)Cl], shows similar activity as cisplatin in the HCT116 (colon) cell line and promising activity in the A2780cis (ovarian) cell line (Table 3). Surprisingly, the ruthenium analogue of **1** (complex **2**) showed no activity up to the highest concentration tested (50 μM).

Table 3. In Vitro Growth Inhibition in the A2780, A2780cis and HCT116 Cell Lines for Compounds **1**−**5** and **7**−**9** and Cisplatin (CDDP) as Control, IC_{50} (μM)[a]

compd	A2780	A2780cis	HCT116
1	24.5 ± 1.0	30.1 ± 0.8	20.2 ± 0.3
2	>50[b]	>50[b]	ND[c]
3	11.8 ± 0.1	7.8 ± 0.4	2.6 ± 0.4
4	21.1 ± 4.6	15.9 ± 0.4	10.3 ± 0.1
5	>50	>50	>50
7	>50	>50	>50
8	>50	>50	>50
9	33.2 ± 0.3	31.9 ± 0.8	22.0 ± 2.5
CDDP	2.36 ± 0.1	16.9 ± 0.5	2.7 ± 0.5

[a] Drug treatment period was 24 h. Each value represents the mean ± SD for three independent experiments. [b] Testing hampered by low aqueous solubility of **2**. [c] ND = not determined

Table 4. Time Dependence of Nucleobase Adduct Formation for Compounds **1**−**5** and **7**−**9** Determined by ^{1}H NMR

compd	time/h	% **9EtG** adduct	% **9EtA** adduct
1	0.17	56	0
	24	56	0
2	0.17	∼34[a]	0
	24	∼34[a]	0
3	0.17	31	0
	24	43	0
4	0.17	57	0
	24	57	0
5	0.17	70	0
	24	75	0
7	0.17	0	0
	24	0	0
8	0.17	0	0
	24	0	0
9	0.17	68	0
	24	68	0

[a] Low solubility caused low signal-to-noise ratio in spectra

Binding to Model Nucleobases 9-Ethyl Guanine (9EtG) and 9-Ethyl Adenine (9EtA). Nucleobase binding reactions using the model compounds 9-ethyl guanine (**9EtG**) and 9-ethyl adenine (**9EtA**; Chart 1) were investigated. Solutions of all arene compounds (1 mM; containing an equilibrium mixture of the chlorido and respective aqua adducts as the major species) with 1 mol equiv of **9EtG** or **9EtA** in D_2O were prepared and ^{1}H NMR spectra were recorded at various time intervals. The percentage of nucleobase binding based on ^{1}H NMR peak integrals is shown in Table 4. The addition of 1 mol equiv **9EtG** to aqueous solutions of *N*,*N*-coordinated compounds **1**−**5** and **9** gave rise to new peaks due to nucleobase adduct formation after ca. 10 min (33−70%, Table 4) with no further changes observed after 24 or 72 h, except for complex **3**, which showed 10% more binding to **9EtG** after 24 h. Compound **2**, the ruthenium analogue of osmium complex **1**, showed reduced nucleobase binding compared to **1**, however due to its low solubility (<1 mM), low signal-to noise ratios were obtained. The addition of 1 mol equiv **9EtA** to aqueous solutions of the *N*,*N*-coordinated compounds resulted in no new peaks even after 72 h. Also the *N*,*O*-coordinated complexes **7** and **8** did not give rise to any new peaks upon reaction with **9EtG** or **9EtA** for 72 h (Table 4).

Computation. The minimum energy structures of nucleobase adducts of *N*,*N*-coordinated compound **1**, [(η^6-*p*-cymene)Os(*N*-2,4-difluoro-Ph-picolinamide)9EtG-*N7*]$^+$ (**1**−**9EtG**), and [(η^6-*p*-cymene)Os(*N*-2,4-difluoro-Ph-picolinamide)9EtA-*N7*]$^+$, (**1**−**9EtA**), and *N*,*O*-coordinated compound

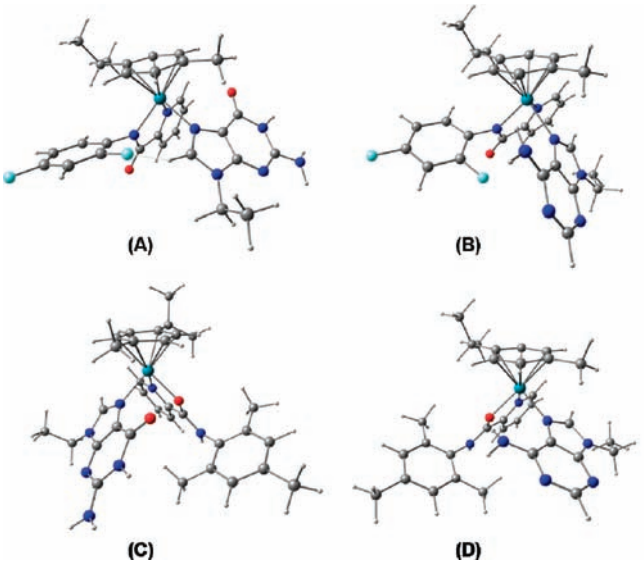

Figure 2. Optimized geometries for the cations (A) [(η^6-*p*-cymene)Os(*N*-2,4-F-Ph-picolinamide)9EtG-*N7*]$^+$ (**1**−**9EtG**), (B) [(η^6-*p*-cymene)Os(*N*-2,4-F-Ph-picolinamide)9EtA-*N7*]$^+$ (**1**−**9EtA**), (C) [(η^6-*p*-cymene)Os(*N*-2,4,6-Me-Ph-picolinamide)9EtG-*N7*]$^{2+}$ (**7**−**9EtG**), and (D) [(η^6-*p*-cymene)Os(*N*-2,4,6-Me-Ph-picolinamide)9EtA-*N7*]$^{2+}$ (**7**−**9EtA**).

Table 5. Gas Phase and Solution (COSMO) **9EtG** and **9EtA** Binding Energies for Complexes **1**−**9EtG**, **1**−**9EtA**, **7**−**9EtG**, and **7**−**9EtA**[a]

	compound	**9EtG** kcal/mol	**9EtA** kcal/mol
1	gas	48.7	31.8
7		65.7	52.9
1	COSMO	64.4	43.3
7		80.4	62.7

[a] Binding energies for structures depicted in Figure 3.

7, [(η^6-*p*-cymene)Os(*N*-2,4,6-trimethyl-Ph-picolinamide)9EtG-*N7*]$^{2+}$ (**7**−**9EtG**), and [(η^6-*p*-cymene)Os(*N*-2,4,6-trimethyl-Ph-picolinamide)9EtA-*N7*]$^{2+}$ (**7**−**9EtA**), obtained from DFT calculations, are shown in Figure 2. The total binding energy of **9EtG** and **9EtA** (see Chart 1 for their structures) in both adducts is shown in Table 5. Both nucleobases show significant binding energies toward both compounds **1** and **7**; the bonding of 9-ethyl guanine is more favorable than for 9-ethyl adenine (by 16.9 kcal/mol and 12.7 kcal/ mol for **1**−**9EtG** and **7**−**9EtG**, respectively). The role of solvation was investigated by calculating the binding energies with COSMO, which simulates aqueous environments. The effect of solvation was similar for all four nucleobase adducts; it is notable that guanine is better solvated (Table 5).

Discussion

Os^{II} and Ru^{II} complexes **1**−**9** (Chart 1) containing *N*-Ph-picolinamide derivatives that can act as *N*,*N*- (through pyridyl and amidinato nitrogen) or *N*,*O*-donors (through the pyridyl nitrogen and carbonyl oxygen) have been synthesized and characterized. In an attempt to understand their contrasting cytotoxic behavior toward cancer cells, we have investigated their aquation rates, the acidity of aqua adducts, and nucleobase binding in relation to the nature of the substituents on the phenyl ring of the picolinamide ligand.

The structures of the complexes depend intimately on electronic effects and steric demands of the functional groups on the phenyl ring of the picolinamide ligand. Electron-withdrawing substituents such as nitro and fluoro groups on the phenyl ring appear to favor coordination through both nitrogens for Os^{II} and Ru^{II}. However, an equilibrium between the two configurations was observed under certain conditions. Variable temperature NMR experiments on a 50:50 mixture of *N*,*N* and *N*,*O* forms of [(η^6-*p*-cym)Os(*N*-2-nitro-Ph-picolinamide)Cl] (**3**) showed that the *N*,*O*-coordinated complex is the kinetic product while *N*,*N*-coordination is thermodynamically favored (Figure S5, SI). Indeed, for compounds **1**−**4** and **9**, neutral monomers containing *N*,*N*-coordination could be obtained. Generally, osmium−nitrogen bonds are more stable than osmium−oxygen bonds. The increased acidity of the amide proton caused by the electron-withdrawing (difluoro and nitro) groups on the phenyl ring for **1**−**4**, facilitates proton loss in solution, favoring *N*,*N*-coordination. Complex **9** does not contain electron-withdrawing substituents on the phenyl ring, but biphenyl as the arene is less electron-rich compared to the *p*-cymene arene present in **1**−**4** and was also isolated as the *N*,*N*-complex. The X-ray crystal structure of active compounds **1** and **3** show weak intermolecular $\pi-\pi$ stacking (Figure S2, SI). Similar $\pi-\pi$ interactions could contribute to the cytotoxicity of these systems involving intercalation into DNA.

The observed *N*,*O*-coordination in compounds **7** and **8**, both of which contain the *N*-2,4,6-trimethyl-Ph-picolinamide ligand, can be explained by the presence of sterically demanding methyl groups, which, in combination with their electron-donating effect (i.e., making the amide proton less acidic), favor *N*,*O*-coordination. A ^{1}H NMR peak for the amide N*H* of both **7** and **8** was observed in their spectra but accompanied by line broadening of all the peaks, suggesting the presence of chemical exchange due to ring-opening and closing; this demonstrates the lability of the Os/Ru−O bonds, something that has previously been observed in acetylacetonate complexes.[23]

The presence of the PF_6^- anion had a directing effect on the configuration of isolated complex **5**. When the product was isolated without NH_4PF_6 addition, a mixture of *N*,*N*- and *N*,*O*-coordinated products was observed. When the PF_6^- anion was present, dimerization of two osmium complexes through H-bridging between the two carbonyl groups of adjacent picolinamide ligands appeared to occur. The bridging proton confers an overall +1 charge, and PF_6^- acts as the counterion. The electron-donating methoxy functional groups may prevent facile amide proton loss in solution to form exclusively the neutral *N*,*N*-coordinated product but do not cause enough steric hindrance (the 6-position on phenyl is still unsubstituted) for the exclusive formation of the *N*,*O*-linkage isomer. In the amide tautomeric form (HO-C=N), the O−H group may associate with another monomer forming the cationic dimeric species in the presence of PF_6^-, creating a binding mode that is intermediate between *N*,*O*- and *N*,*N*-coordination. This unusual motif also appears to be present in the X-ray crystal structure of ruthenium analogue **6** ([**6-H-6**]$\mathbf{PF_6}$, Figure 1C) and in complex **10**, ([(η^6-*p*-cym)Ru(*N*-2-fluoro-Ph-picolinamide)Cl]$_2$HPF$_6$, [**10-H-10**]$\mathbf{PF_6}$, Figure S3, SI), where the H atom in the O−H−O motif was located in the Fourier map resulting in a linear O−H−O bond. A similar motif has been reported for [Cu{6,6′-bis(2-hydroxyphenyl)-2,2′-bipyridine}](HPF)$_{0.5}\cdot$H$_2$O,[24] where the O···O distance is 2.397 Å and the O−H−O angle almost linear at 173.85°. In the case of complex **6**, the O7···O7′ distance is 2.425 Å. A

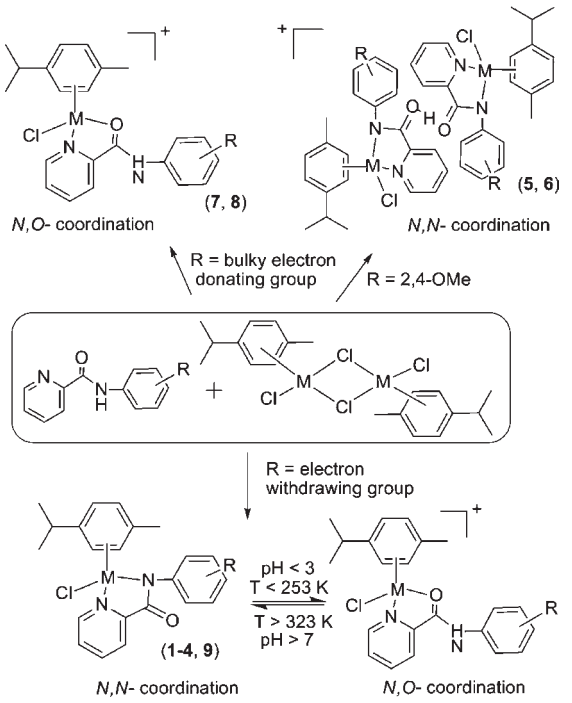

Figure 3. Summary of reaction pathways giving rise to *N*,*N*- or *N*,*O* coordination for osmium and ruthenium (M = Os or Ru) picolinamide complexes.

summary of the different reaction pathways which could give rise to *N*,*N*- or *N*,*O*-coordinated osmium and ruthenium picolinamide complexes is presented in Figure 3.

Dynamic NMR studies on a 50:50 mixture of the two configurational isomers of compound **3** showed that the equilibrium between the *N*,*O*- and *N*,*N*-coordination is temperature- as well as pH-dependent. At low temperatures, the kinetic *N*,*O*-coordinated product remained as 50% of the mixture, while the thermodynamic *N*,*N*-coordinated product was exclusively and irreversibly formed at a temperature of 323 K or higher (Figure S5, SI). Changing the pH of the same mixture of linkage isomers to an acidic pH* of 2 resulted in the formation of only the *N*,*O*-coordinated product. Under acidic conditions, the amide nitrogen remains protonated, favoring donation through the lone pairs of oxygen. Surprisingly, even at pH 2.4, the equilibrium mixture contained some of the thermodynamic *N*,*N*-coordinated product. Full, reversible, conversion to the *N*,*N*-form was observed over the pH range of 7.1−8.6 (Figure S6, SI). These observations show the high thermodynamic stability of the *N*,*N*-coordinated linkage isomer and suggest the possibility that appropriate ligand design could allow controllable switching between *N*,*O* and *N*,*N* configurations under biological conditions.

Previous studies on the hydrolysis rates of Os^{II} arene compounds of the type $[(\eta^6\text{-arene})Os(XY)Cl]^{n+}$ where XY is a *N*,*N*-coordinated chelating ligand gave an aqueous half-life of 6.4 h for XY = ethylenediamine, ca. 40 times slower than for its ruthenium analogue.[25] The rate of hydrolysis was slowed down even further (by a factor of ca. 7) by incorporating a π-acceptor chelating ligand such as 2,2′-bipyridine or 1,10-phenanthroline as XY.[26] In the present study, however, in which the *N*,*N*-coordinated ligand is anionic, the *N*,*N*-coordinated compounds displayed very fast hydrolysis rates, too fast to measure by ^{1}H NMR even at 288 K ($t_{1/2} \leq 0.12$ h, Table 1). In contrast, the *N*,*O*-coordinated compounds **7** and **8** hydrolyzed comparatively slowly, in the case of Os^{II} arene complex **7**, over 36 times slower at 288 K compared to the *N*,*N*-coordinated compounds **1**−**5** and **9** (Table 1). Therefore, the coordinated chelating ligand can play a major role in controlling the reactivity of these types of complexes.

The substituents on the phenyl ring of the picolinamide ligand may also play a role in their aqueous reactivity. However, all the *N*,*N*-coordinated Os compounds hydrolyzed rapidly and reacted with nucleobases to a similar extent. This appears to be the case regardless of the electronic and steric nature of the substituents on the phenyl ring. The difference observed in the hydrolysis rates can be explained by the strong donor character of the amidate nitrogen and by the overall positive charge on **7** and **8**, which hinders chloride release compared to the neutral *N*,*N*-coordinated complexes **1**−**5** and **9**. Indeed, in the X-ray crystal structures, the Os−Cl bond in **7** is 0.06 Å shorter than the Os−Cl bond in complex **1** (Table S2, SI). Changing Os^{II} in **7** to Ru^{II} (**8**) increased the aqueous reactivity (~10 times, Table 1), in line with the generally faster kinetics observed for the second row Ru compared to the third row Os transition metal.

The *N*,*O*-coordinated compounds **7** and **8** and *N*,*N*-coordinated complex **5** were noncytotoxic up to the highest concentration tested (50 μM). The difference between **5** and the other *N*,*N*-coordinated compounds is that it contains strong electron-donating substituents on the phenyl ring, whereas the other *N*,*N*-coordinated compounds (**1**−**4**) contain electron-withdrawing substituents. The strong donating capabilities of the methoxy substituents is demonstrated by the protonation of the carbonyl oxygen and formation of the hydrogen bridged dimer in the crystal structure of **6**, the Ru analogue of **5** (Figure 1C). Such protonation may weaken the metal−N bond and make the complex susceptible to reactions with other biomolecules in cells. In the case of complexes **7** and **8**, their slow aqueous reactivity might prevent the complexes reacting with targets such as, DNA. Promising activity was observed for the neutral *N*,*N*-coordinated compounds **1**, **3**, **4**, and **9** in the HCT116 (colon), A2780 (ovarian), and A2780cis (ovarian, cisplatin resistant) cell lines (Table 3, Figure S8, SI). A trend in cytotoxic activity was observed in all three cell lines: electron-withdrawing substituents (F, NO_2) on the uncoordinated phenyl ring influence the biological activity significantly, with activity decreasing in the order of **3** ≫ **4** > **1** > **9** (where **9** has an unsubstituted phenyl ring, Chart 1). The activity of **9** is probably enhanced by the presence of biphenyl as the coordinated arene instead of *p*-cymene, which is the arene in the other compounds because biphenyl can act as a DNA intercalator, contributing to its cytotoxicity.[27−29] Complex **3**, $[(\eta^6\text{-}p\text{-cym})Os(N\text{-4-nitro-Ph-picolinamide})Cl]$, shows similar activity as cisplatin in the HCT116 (colon) cell line and shows promising activity in the A2780 (ovarian) cisplatin resistant cell line (Table 3). The different cytotoxicity profiles of the four active compounds indicate that the nature of the substituent is important in the mechanism of action of these complexes. In addition, the difference in cytotoxicity observed between isomers **4** (*o*-NO_2) and **3** (*p*-NO_2) indicates that also the position of the substituent on the phenyl ring is important for the cytotoxic activity of these complexes. Complex **2** (the ruthenium analogue of **1**) appears to be nontoxic, however its low solubility hampered the testing.

Binding studies of Ru^{II} and Os^{II} arene complexes with nucleobases are of special interest because DNA is considered to be the main target for classical transition-metal anticancer drugs.[30] Distortions of DNA structure are critical for protein recognition and downstream processing and often correlate

with anticancer activity.[31,32] To gain insight into the reactivity of these types of complexes with DNA, the nucleobase derivatives 9-ethyl guanine (**9EtG**) and 9-ethyl adenine (**9EtA**) were used as models (Chart 1). Previously we found that the Os^{II} biphenyl complex containing the *N*,*N*-chelator ethylenediamine (en) as ligand reacted only slowly with **9EtG** and only to a limited extent with adenosine (Ado).[25] All neutral *N*,*N*-coordinated compounds studied in this work (**1**−**4** and **9,** Chart 1) showed significant and rapid binding to **9EtG** (detectable after just 10 min; 32−70%, Table 4). The cytotoxic activity of these complexes might therefore be aided by their fast reaction with guanine bases in the target DNA. Surprisingly, inactive compound **5**, containing ortho and para methoxy substituents on the phenyl ring of the chelating ligand, also binds to **9EtG** to a large extent, suggesting that its inactivity is not due to its reactivity toward DNA but perhaps due to inactivating side reactions with other biomolecules or possibly reduced cell uptake due to its different charge distribution. However, we cannot rule out the possibility that DNA is not the primary target for these types of complexes. Ruthenium complex **2**, the analogue of the active osmium complex **1**, appeared to show reduced nucleobase binding compared to **1** (Table 4), however NMR studies were hampered by its low solubility. None of the active cytotoxic *N*,*N*-coordinated compounds nor inactive complex **5** showed any binding toward 9-ethyl adenine, a similar preference to that observed for the ethylenediamine Os^{II} arene complexes mentioned earlier. *N*,*O*-coordinated complexes **7** and **8** did not bind to the guanine or adenine model nucleobases. This is attributable to their kinetic inertness and suggests that they would not be effective in targeting DNA. Bar charts that summarize the effect of *N*,*N*- versus *N*,*O*-binding on the hydrolysis rates, guanine and adenine binding, and cytotoxic activity of compounds **1**, **3**, **4** and **7**−**9** are shown in Figure 4.

Computational methods were used to gain insight into the guanine-specific binding observed for compounds **1**−**5** and **9** and the lack of nucleobase reactivity for compounds **7** and **8** (Chart 1, Table 5). The total bonding energies in the gas phase and with water solvation (COSMO) of the nucleobases 9-ethyl guanine (**9EtG**) and 9-ethyl adenine (**9EtA**, Chart 1) in the optimized structures of $[(\eta^6\text{-}p\text{-cymene})Os(N\text{-}2,4\text{-difluoro-Ph-picolinamide})9EtG\text{-}N7]^+$ (**1**−**9EtG**), $[(\eta^6\text{-}p\text{-cymene})Os(N\text{-}2,4\text{-difluoro-Ph-picolinamide})9EtA\text{-}N7]^+$ (**1**−**9EtA**), $[(\eta^6\text{-}p\text{-cymene})Os(N\text{-}2,4,6\text{-trimethyl-Ph-picolinamide})9EtG\text{-}N7]^{2+}$ (**7**−**9EtG**), and $[(\eta^6\text{-}p\text{-cymene})Os(N\text{-}2,4,6\text{-trimethyl-Ph-picolinamide})9EtA\text{-}N7]^{2+}$ (**7**−**9EtA**) (see Figure 2 for their structures) are shown in Table 5. The **9EtG** nucleobase adduct of active compound **1** (**1**−**9EtG**) is thermodynamically preferred by 16.9 kcal mol^{-1} compared to the **9EtA** adduct of **1** (**1**−**9EtA**), with a bonding energy of 48.7 kcal mol^{-1} compared to 31.8 kcal mol^{-1} for the adenine adduct (Table 5). This significant difference may explain the guanine-specific binding observed for the neutral *N*,*N*-coordinated compounds **1**−**5** and **9**. Surprisingly, inactive compound **7** displays high bonding energies toward both nucleobases, showing a similar thermodynamic preference for guanine over adenine by 12.7 kcal mol^{-1}, with a bonding energy of 65.7 kcal/mol for 7−**9EtG** compared to 52.9 kcal/mol for **7**−**9EtA** (Table 5). The high bonding energies calculated for both nucleobase adducts of **7** indicate that its observed inactivity toward the nucleobases is not due to the thermodynamic stability of the nucleobase adducts but most likely due to high kinetic barriers. Because nucleobase binding is likely to require initial aquation, the slow hydrolysis rates of **7** and **8** will presumably hinder nucleobase binding. The high nucleobase bonding energies found for **7** cannot be attributed to a difference in solvation effects for **1** and **7** (which are differently charged, +1/+2, respectively) because the solvation effects calculated using COSMO to simulate aqueous conditions are similar for both nucleobase adducts of **1** and **7**. Guanine is notably more strongly solvated (Table 5). This higher solvation energy for guanine (4.2 kcal mol^{-1} and 5.0 kcal mol^{-1} higher than **9EtA** for **1** and **7,** respectively) can be attributed to the high charge concentration at the oxo group in guanine.

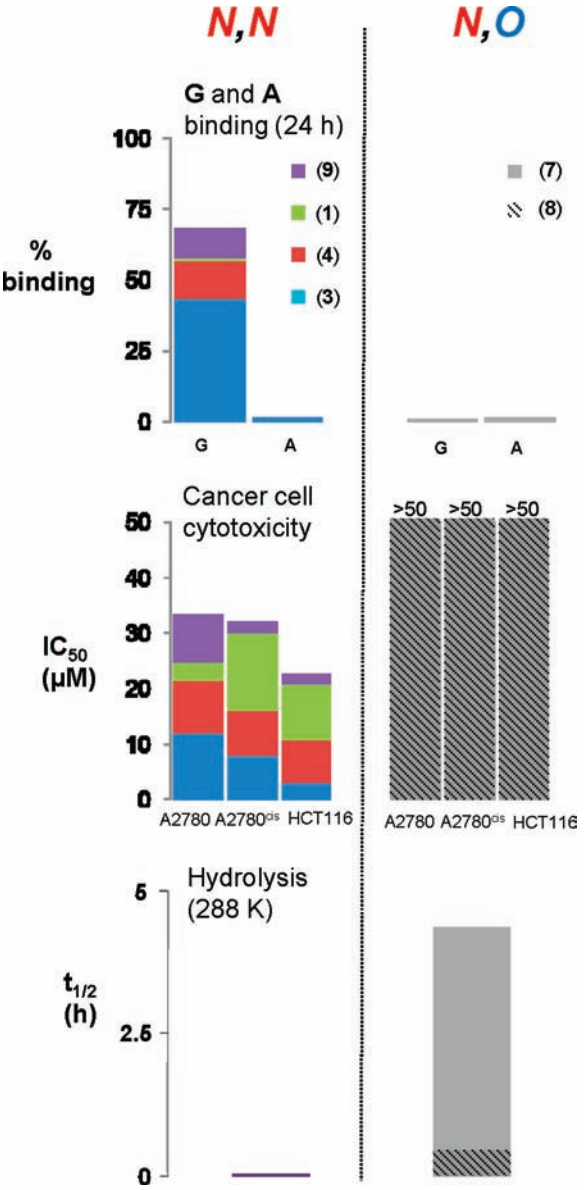

Figure 4. Bar chart illustrating the effect of *N*,*N*- versus *N*,*O*-binding of picolinamide on the hydrolysis rates, guanine and adenine binding, and cytotoxic activity in A2780 (ovarian), A2780cis (ovarian cisplatin resistant), and HCT116 (colon) cancer cell lines, of complexes **1**, **3**, **4**, **7**, **8**, and **9**.

Conclusions

This study demonstrates that the coordination mode (*N*,*N* versus *N*,*O*) and substituents on the phenyl ring of *N*-phenylpicolinamide ligands in both Ru^{II} and Os^{II} arene complexes can have a dramatic effect on the aqueous and biological

activity of the complexes. Both *N*,*N*- and *N*,*O*-configurations were characterized for both metals and are determined by electronic effects and steric demands of the functional groups on the phenyl ring of the picolinamide ligand. In addition, an unusual binding mode, involving protonation of the amidinato carbonyl, was observed in the *N*,*N*-complexes **5** and **6** (see Figure 3 for a summary). Depending on the synthetic method, an equilibrium between the *N*,*O*- and *N*,*N*-coordinated products was obtained that is time and temperature- (irreversible) as well as pH-dependent (reversible). This suggests that appropriate ligand design could be used to optimize the interconversion between these two coordination modes under biological conditions.

In contrast to complexes in the family containing neutral *N*, *N* donors $[(\eta^6\text{-arene})Os(XY)Cl]^+$, where XY is ethylenediamine, 2,2′-bipyridine, or 1,10-phenanthroline, all the *N*,*N*-coordinated picolinamide compounds in this study, displayed rapid hydrolysis rates ($t_{1/2} \leq 0.12$ h). The *N*,*O*-coordinated compounds **7** and **8** hydrolyzed much more slowly, over 36 times slower for **7** (at 288 K) than the *N*,*N*-coordinated compounds (**1**−**5** and **9**). This large difference in aqueous reactivity between complex **7** and complexes **1**, **3**, **4**, and **9** is remarkable and demonstrates not only the importance of the chelating ligand in these complexes but also suggests that these complexes can be "tuned" to obtain biologically favorable ligand exchange rates.

Promising cytotoxic activity for Os^{II} complexes followed the order **3** ≫ **4** > **1** > **9** in all three cell lines tested, and compound **3** shows similar activity as cisplatin in HCT116 (colon) cell line and shows promising activity in the A2780cis (ovarian cisplatin resistant) cell line.

All active compounds showed significant binding to **9EtG** with 32−70% binding after just 10 min. Their rapid binding to guanine may aid binding to DNA and contribute to their cytotoxicity. No binding to adenine (**9EtA**) was observed for any of the active compounds. *N*,*O*-coordinated complexes **7** and **8** did not show any binding to guanine or adenine model nucleobases, indicating that their cytotoxic inactivity is likely to be due to their overall slow kinetics, hindering their binding to DNA. The anomalous behavior of *N*,*N*-complex **5**, which binds rapidly to 9-ethylguanine but is noncytotoxic, seems likely to be due to the presence of the electron-donating methoxy groups on the phenyl ring and high basicity of the carbonyl oxygen, which was partially protonated in the crystal structure of the isolated dimer. In DFT calculations, the **9EtG** nucleobase adduct of active complex **1** is thermodynamically preferred compared to its **9EtA** adduct by 16.9 kcal mol^{-1} (Table 5), explaining the guanine-specific binding observed experimentally for all the *N*,*N*-coordinated compounds (**1**−**5** and **9**). Surprisingly, DFT calculations with inactive compound **7** show high bonding energies toward both nucleobases. This indicates that its unreactivity toward both nucleobases is most likely caused by high kinetic barriers, as indicated by its slow hydrolysis rate.

On the basis of the examples studies here, it appears that *N*, *N*- and *N*,*O*-coordinated *N*-phenyl picolinamide Os^{II} and Ru^{II} arene complexes can exhibit dramatic differences in their biological reactivity. The *N*,*N*-coordinated compounds hydrolyze quickly, show selective binding to guanine, and exhibit cancer cell cytotoxicity, while the *N*,*O*-coordinated compounds hydrolyze slowly, display no reactivity toward guanine or adenine, and are noncytotoxic, as summarized in Figure 4.

Experimental Section

Materials. 1,4-Dihydrobiphenyl and the dimers, $[(\eta^6\text{-}p\text{-cym})Os/RuCl_2]_2$ and $[(\eta^6\text{-bip})OsCl_2]_2$, were prepared by previously reported procedures.[25,33] 9-Ethyl guanine and 9-ethyl adenine were purchased from Sigma-Aldrich. $OsCl_3 \cdot nH_2O$ and $RuCl_3 \cdot nH_2O$ were purchased from Alfa Aesar. All deuterated solvents were obtained from Aldrich. Ethanol and methanol were distilled over magnesium/iodine prior to use. Complexes **1**−**10** were synthesized from the dimeric precursors, $[(\eta^6\text{-}p\text{-cym})MCl_2]_2$ (where M is Os or Ru) and $[(\eta^6\text{-bip})OsCl_2]_2$, using procedures similar to those reported previously for other half-sandwich arene complexes.[34,35] The purities of compounds **1**−**10** were all determined to be ≥95% by elemental analysis and are reported in the SI. In addition, ^1H, ^{13}C NMR, and ESI-MS data for compounds **1**−**10** and the preparations and characterization data for the *N*-Ph-picolinamide ligands are in the SI.

Preparation of the Complexes: [(η⁶-*p*-cym)Os(*N*-2,4-difluoro-Ph-picolinamide)Cl] (1). A suspension of $[(\eta^6\text{-}p\text{-cym})OsCl_2]_2$ (51 mg, 0.086 mmol) and *N*-2,4-difluoro-Ph-picolinamide (2 equiv, 32 mg) in dry and degassed EtOH (25 mL) was refluxed under argon for 2 h, after which time the solution had turned color from brown to yellow. The solution was filtered while hot into a filtered solution of NH_4PF_6 (∼5 mol equiv, 110 mg) in 5 mL of EtOH. This mixture was stirred for another hour at ambient temperature. The filtrate was brought to dryness on a rotary evaporator, and the orange solid was redissolved in a minimum of dichloromethane; excess of the PF_6^- salt formed a white precipitate. This was filtered off and the volume of the filtrate reduced on a rotary evaporator until an orange precipitate began to form. The mixture was left standing at 278 K to allow precipitation to occur. The orange crystalline powder was recovered by filtration and air-dried to give a final yield of 42.9 mg (56%) Crystals of **1** suitable for X-ray diffraction were obtained by slow evaporation from MeOH at ambient temperature.

[(η⁶-*p*-cym)Ru(*N*-2,4-difluoro-Ph-picolinamide)Cl] (2). A suspension of *N*-2,4-difluoro-Ph-picolinamide (75 mg, 0.32 mmol) was added to a Schlenk tube containing a stirred solution of $[(\eta^6\text{-}p\text{-cym})RuCl_2]_2$ (0.1 g, 0.16 mmol) in dry ethanol (50 mL). The mixture was warmed at 323 K for 15 min until dissolution and then filtered over NH_4PF_6 (0.1 g, excess). The mixture was stirred under dinitrogen for 18 h to give an orange solution. The solvent was removed in vacuo to leave an orange solid. The solid was washed with petrol (3 × 10 mL) and dried in vacuo to give an orange powder. The product was dissolved in MeOH for recrystallization. Red−orange prism-shaped crystals were isolated, washed in petrol (3 × 10 mL), and dried in vacuo, Yield: 56 mg (68.8%). Crystals of **2** suitable for X-ray diffraction were obtained by slow evaporation from MeOH at ambient temperature.

[(η⁶-*p*-cym)Os(*N*-4-nitro-Ph-picolinamide)Cl] (3). A suspension of $[(\eta^6\text{-}p\text{-cym})OsCl_2]_2$ (52.7 mg, 0.087 mmol) and *N*-4-nitro-Ph-picolinamide (2.1 mol equiv, 35.5 mg) in dry and degassed EtOH (25 mL) was refluxed mildly for 3 h, after which no significant color change was observed. The solution was filtered while hot into a filtered solution of NH_4PF_6 (∼5 mol equiv, 110 mg) in 5 mL of EtOH. This mixture was stirred for another 2 h at ambient temperature. The orange solution was reduced in volume on a rotary evaporator until an orange precipitate began to form. The mixture was left standing at 278 K to allow further precipitation. The orange crystals were recovered by filtration and air-dried to give a final yield 15.3 mg (19%). Crystals of **3**·MeOD suitable for X-ray diffraction were obtained by slow evaporation from MeOD at ambient temperature.

[(η⁶-*p*-cym)Os(*N*-2-nitro-Ph-picolinamide)Cl] (4). A suspension of $[(\eta^6\text{-}p\text{-cym})OsCl_2]_2$ (50 mg, 0.083 mmol) and *N*-2-nitro-Ph-picolinamide (2 mol equiv, 35 mg) in dry and degassed EtOH (25 mL) was refluxed for 2 h, after which no significant color change was observed. The solution was filtered while hot into a filtered solution of NH_4PF_6 (∼5 mol equiv, 110 mg) in 5 mL of

EtOH. This mixture was stirred for another 2 h at ambient temperature. The solvent was removed on a rotary evaporator and the residue redissolved in dichloromethane. This mixture was filtered, and again the solvent was removed on a rotary evaporator. The orange solid was redissolved in a minimum of MeOH and was left standing at 278 K to allow precipitation to occur. The orange crystals were recovered by filtration and air-dried to give a final yield 27.5 mg (36%).

[(η^6-*p*-cym)Os(*N*-2,4-dimethoxide-Ph-picolinamide)Cl]$_2$PF$_6$ (5). A suspension of [(η^6-*p*-cym)OsCl$_2$]$_2$ (50 mg, 0.081 mmol) and *N*-2,4-dimethoxide-Ph-picolinamide (2 mol equiv, 34 mg) in dry and degassed EtOH (25 mL) was refluxed for 2.5 h, after which no significant color change was observed. The solution was filtered while hot into a filtered solution of NH_4PF_6 (~5 mol equiv, 110 mg) in 5 mL of EtOH. This mixture was stirred for another hour at ambient temperature. An orange precipitate formed in this period. The volume was reduced on a rotary evaporator upon which more precipitate began to form. The orange powder was recovered as two associating monomers with PF_6 as a counterion by filtration and air-dried to give a final yield of 57.6 mg (74%).

[(η^6-*p*-cym)Ru(*N*-2,4-dimethoxide-Ph-picolinamide)Cl]$_2$PF$_6$ (6). *N*-2,4-Dimethoxide-Ph-picolinamide (0.083 g, 0.32 mmol) was added to a Schlenk tube containing a stirred solution of dichloro-*p*-cymene ruthenium dimer (0.1 g, 0.16 mmol) in dry ethanol (50 mL). The mixture was warmed at 323 K for 15 min until dissolution and then filtered over to NH_4PF_6 (0.1 g, excess). The mixture was stirred under nitrogen for 18 h to give an orange solution. The solvent was removed in vacuo to leave an orange solid. The solid was washed with petrol (3 × 10 mL) and dried in vacuo to give an orange powder. The product was dissolved in MeOH for recrystallization. The coffin shaped crystals were suitable for X-ray crystallographic analysis (0.053 g, 0.044 mmol, 55%).

[(η^6-*p*-cym)Os(*N*-2,4,6-trimethyl-Ph-picolinamide)Cl]PF$_6$ (7). A suspension of [(η^6-*p*-cym)OsCl$_2$]$_2$ (50 mg, 0.083 mmol) and *N*-2,4,6-trimethyl-Ph-picolinamide (2 mol equiv, 29.9 mg) in dry and degassed EtOH (25 mL) was refluxed under argon for 2 h, after which the solution turned color from brown to bright yellow. The solution was filtered while hot into a filtered solution of NH_4PF_6 (~5 mol equiv, 110 mg) in 5 mL of EtOH. This mixture was stirred for another half hour at ambient temperature. The filtrate was brought to dryness on a rotary evaporator, and the yellow solid was redissolved in a minimum of dichloromethane; excess of the PF_6 salt formed a white precipitate. This was filtered off and the volume of the filtrate was reduced on a rotary evaporator until an orange precipitate began to form. The mixture was left standing at 278 K to allow precipitation to occur. The orange crystals were recovered by filtration and air-dried to give a final yield of 59 mg (78%). Crystals of **7**·CH_2Cl_2 suitable for X-ray crystallography were obtained by slow evaporation from CH_2Cl_2 at ambient temperature.

[(η^6-*p*-cym)Ru(*N*-2,4,6-trimethyl-Ph-picolinamide)Cl]PF$_6$ (8). A suspension of [(η^6-*p*-cym)RuCl$_2$]$_2$ (78 mg, 0.127 mmol) and *N*-2,4,6-trimethyl-Ph-picolinamide (2 equiv, 67 mg) in dry and degassed EtOH (25 mL) was refluxed under argon for 2.5 h. The orange solution was filtered while hot into a filtered solution of NH_4PF_6 (~5 equiv, 110 mg) in 5 mL of EtOH. This mixture was stirred for 16 h at ambient temperature. The orange solution was reduced in volume on a rotary evaporator until an orange precipitate began to form. The mixture was left standing at 278 K to allow further precipitation. The orange crystals were recovered by filtration and air-dried to give a final yield 56 mg (69%). Crystals of **8**·$CHCl_3$ suitable for X-ray crystallography were obtained by slow evaporation from ethanol at ambient temperature.

[(η^6-bip)Os(*N*-Ph-picolinamide)Cl] (9). A suspension of [(η^6-bip)OsCl$_2$]$_2$ (50 mg, 0.087 mmol) and *N*-Ph-picolinamide (2 mol equiv, 25 mg) in dry and degassed EtOH (25 mL) was refluxed under argon for 1 h. The brown solution was filtered while hot into a filtered solution of NH_4PF_6 (~5 mol equiv, 110 mg) in 5 mL of EtOH. This mixture was stirred for another 3 h at ambient temperature. The mixture was reduced in volume on a rotary evaporator until a precipitate began to form and was left standing at 278 K. The orange crystalline powder was recovered as two associating monomers with PF_6 as a counterion by filtration and air-dried to give a final yield of 44.4 mg (64%).

[(η^6-*p*-cym)Os(*N*-2-fluoro-Ph-picolinamide)Cl] (10). *N*-2-Fluoro-Ph-picolinamide (0.069 g, 0.32 mmol) was added to a Schlenk tube containing a stirred solution of dichloro-*p*-cymene ruthenium dimer (0.1 g, 0.16 mmol) in dry ethanol (50 mL). The mixture was warmed at 323 K for 15 min until dissolution and then filtered over to NH_4PF_6 (0.1 g, excess). The mixture was stirred under dinitrogen for 18 h to give an orange solution. The solvent was removed in vacuo to leave an orange solid. The solid was washed with petrol (3 × 10 mL) and dried in vacuo to give an orange powder. The product was dissolved in MeOH for recrystallization. Red−orange prism-shaped crystals were isolated, washed in petrol (3 × 10 mL), and dried in vacuo. The crystals were suitable for X-ray crystallographic analysis (0.060 g, 0.054 mmol, 67.1%).

Methods and Instrumentation: NMR Spectroscopy. ^{1}H NMR spectra were acquired in 5 mm NMR tubes at 298 K (unless stated otherwise) on either a Bruker DMX 500 (^{1}H = 500.13 MHz) or AVA 600 (^{1}H = 599.81 MHz) spectrometer. ^{1}H NMR chemical shifts were internally referenced to (CHD_2)(CD_3)SO (2.50 ppm) for DMSO-d_6, $CHCl_3$ (7.26 ppm) for chloroform-d_1, CD_2HOD (3.34 ppm) for methanol-d_4, and to 1,4-dioxane (3.75 ppm) for aqueous solutions. For NMR spectra recorded for aqueous solutions, water suppression was carried out using Shaka or presaturation methods.[36] All data processing was carried out using TOPSPIN version 2.0 (Bruker U.K. Ltd.).

Elemental Analysis. Carbon, hydrogen, and nitrogen (CHN) elemental analysis were carried out at The University of St. Andrews in the School of Chemistry on a Carlo Erba CHNS analyzer or by Warwick Analytical Service using an Exeter analytical elemental analyzer (CE440) and the School of Chemistry Microanalytical Service, University of Leeds. Mass spectra were obtained on a VG Autospec mass spectrometer by the Department of Chemistry Mass Spectrometry Service, University of Leeds.

X-ray Crystallography. Diffraction data for **1** and **3** were collected by the EPSRC National Crystallography Service (Southampton) using a Bruker-Nonius FR591 anode X-ray generator and a Bruker-Nonius Kappa CCD area detector. The crystal was held at 120(2) K with an Oxford Cryosystem cryostream cooler.[37] Absorption corrections for all data sets were performed with the multiscan procedure SADABS;[38] structures were solved using either Patterson or direct methods (SHELXL[39] or DIRDIF[40]); complexes were refined against F or F^2 using SHELXTL, and H-atoms were placed in geometrically calculated positions. X-ray diffraction data for **7** were collected with Mo Kα radiation on a Bruker SMART Apex diffractometer equipped with an Oxford Cryosystems low-temperature device operating at 150 K. Following application of a multiscan correction for systematic errors (SADABS[38]), the structure was solved by direct methods (SIR92[41]) and refined by full-matrix least-squares against F^2 (CRYSTALS[42]). H atoms were placed geometrically and then refined subject to distance restraints and finally constrained to ride on their host atoms for the final cycles of refinement. All non-H atoms were refined with anisotropic displacement parameters. The modeling program Diamond 3.020 was used for production of graphics.

X-ray diffraction data for **2**, **6**, **8**, and **10** were collected with a Nonius KappaCCD area-detector diffractometer using graphite monochromated Mo Kα radiation (λ = 0.71073 Å). The crystal was cooled to 150 K by an Oxford Cryosystems low temperature device[37] before data collection using 1.0° φ rotation frames. The images were processed using the DENZO and SCALEPACK programs,[43] followed by structure solution by direct methods

via one of the SHELXS86[44] SIR92,[41]or SIR97[45] programs. All structures were refined by full-matrix least-squares on F^2 using SHELXL97.[39] Molecular graphics were plotted using POVray[46] via XSeed.[47] All non-hydrogen atoms were refined anisotropically. Hydrogen atoms were constrained with a riding model; U(H) was set at 1.2× (1.5× for methyl groups) U_{eq} for the parent atom. There were disorder problems involving solvent of crystallization in the structures of **2** and **8**, and details are given below.

In the case of **2**, the methyl and isopropyl groups (involving C1, C2, C3, C7, and C13) of the *p*-cymene ligand to Ru1 exhibit large ADPs, indicating that the *p*-cymene arene as a whole is displaying some disorder, but this behavior was not modeled. This disorder results in some bond length and angle anomalies in the *p*-cymene arene. For **8**, the severe disorder in the PF_6^- anion could not be resolved, resulting in high anisotropic thermal parameters. In addition, the methyl and isopropyl groups (involving C20, C27, C28, and C29) of the *p*-cymene arene to Ru1 exhibit large ADPs. This indicates that the *p*-cymene ligand as a whole is displaying some disorder, but this behavior was not modeled.

X-ray crystallographic data for compounds **1**, **2**, **3**, **6**, **7**, **8**, and **10** have been deposited in the Cambridge Crystallographic Data Centre under the accession numbers CCDC 708837, 723343, 733992, 723341, 723344, 723340, and 723342, respectively.

pH* Measurements. pH* values (pH meter reading from D_2O solution without correction for effects of D on glass electrode) of NMR samples in D_2O were measured at ca. 298 K directly in the NMR tube, before and after recording NMR spectra, using a Corning 240 pH meter equipped with a micro combination electrode calibrated with Aldrich buffer solutions of pH 4, 7, and 10.

Hydrolysis. The kinetics of hydrolysis of complexes **1**−**5** and **7**−**9** were followed by ^{1}H NMR at 288 K. For this, solutions of the complexes with a final concentration of 0.8 mM in 5% MeOD-d_4/95% D_2O (v/v) were prepared by dissolution of the complexes in MeOD-d_4, followed by rapid dilution using D_2O (pH* of ca. 7). ^{1}H NMR spectra were recorded after various intervals using the presaturation method. The rate of hydrolysis was determined by fitting plots of concentrations (determined by ^{1}H NMR peak integrals) versus time to a pseudo-first-order rate equation using ORIGIN version 5.0 (Microcal Software Ltd.).

pK_a* Calculations. For determinations of pK_a* values (pK_a values for solutions in D_2O), the pH* values of the aqua complexes of **1** and **7** in D_2O (formed in situ by dissolution of the parent chloro complexes) were varied from ca. pH* 2−10 by the addition of dilute NaOD and HNO_3 and ^{1}H NMR spectra were recorded. The chemical shifts of the arene ring protons were plotted against pH*. The pH* titration curves were fitted to the Henderson−Hasselbalch equation, with the assumption that the observed chemical shifts are weighted averages according to the populations of the protonated and deprotonated species. These pK_a* values can be converted to pK_a values by use of the equation pK_a = 0.929pK_a* + 0.42, as suggested by Krezel and Bal,[48] for comparison with related values in literature.

Cancer Cell Cytotoxicity. After plating, human ovarian A2780 and cisplatin-resistant A2780cis cancer cells were treated with Os^{II} and Ru^{II} complexes on day 3, and human colon HCT116 cancer cells on day 2, at concentrations ranging from 0.1 to 100 μM. Solutions of the Os^{II} complexes were made up in 0.125% DMSO to assist dissolution (0.03% final concentration of DMSO per well in the 96-well plate). Cells were exposed to the complexes for 24 h, washed, supplied with fresh medium, allowed to grow for three doubling times (72 h), and then the protein content measured (proportional to cell survival) using the sulforhodamine B (SRB) assay.[49]

Interactions with Nucleobases. The reactions of **1**−**5** and **7**−**9** with model nucleobases typically involved addition of a solution containing 1 mol equiv of nucleobase in D_2O to an equilibrium solution of the complex in D_2O (> 90% aqua). The pH* value of the sample was adjusted if necessary so as to remain close to 7.4 (physiological). ^{1}H NMR spectra of these solutions were recorded at 298 K after various time intervals. In between, the samples were kept at 310 K.

Computation. DFT calculations were carried out using the Amsterdam density functional (ADF)[50] program (version 2007.01). The coordinates of complexes used for the calculations were directly obtained from the X-ray crystal structures. Modifications to the structures were performed in Chemcraft (version 1.5). Geometries and energies were obtained by using the Perdew−Wang gradient-corrected functional (GGA) with scalar ZORA relativistic correction.[51−55] The general numerical integration was 4.0. The frozen core approximation[56] was applied using triple-ζ plus polarization (TZP) basis sets. Default convergence criteria were applied for self-consistent fields (SCF) and geometry optimization. Geometry and energies were confirmed with frequency calculations. The conductor-like screening model (COSMO), as implemented in the ADF program, was used to simulate aqueous environments with ε = 78.4 and a probe radius = 1.9 Å. The atomic radii used were Os = 1.958, F = 1.425, Cl = 1.725, Br = 1.850, O = 1.517, N = 1.608, C = 1.700, and H = 1.350. Single-point calculations were carried out for the guanine and adenine fragments of the cations of complexes **1**−**9EtG** [(η^6-*p*-cymene)Os(*N*-2,4-difluoro-Ph-picolinamide)-9EtG-*N*7]$^+$, **1**−**9EtA** [(η^6-*p*-cymene)Os(*N*-2,4-difluoro-Ph-picolinamide)9EtA-*N*7]$^+$, **7**−**9EtG** [(η^6-*p*-cymene)Os(*N*-2,4,6-trimethyl-Ph-picolinamide)9EtG-*N*7]$^{2+}$, and **7**−**9EtA** [(η^6-*p*-cymene)Os(*N*-2,4,6-trimethyl-Ph-picolinamide)9EtA-*N*7]$^{2+}$ and the fragments without **9EtG** and **9EtA**. The energies of the separate fragments were subtracted from the energy of the entire cations of complexes **1**−**9EtG**, **1**−**9EtA**, **7**−**9EtG**, and **7**−**9EtA** in the single point calculation of all complexes to obtain the total binding energy of **9EtG** and **9EtA** for both complexes.

Acknowledgment. We thank EPSRC National Crystallography Service (University of Southampton) for collecting the diffraction data for complex **1** and **3** and Dr. Michael Khan and Dr. Ana Pizarro (Warwick University) for help and advice on cell culture. This research was supported by the Engineering and Physical Sciences Research Council (EPSRC) and Science City (Advantage West Midlands/ European Regional Development Fund). We also acknowledge our participation in the EU COST Action D39, which enabled us to exchange regularly the most recent ideas in the field of anticancer metallodrugs with several European colleagues.

Supporting Information Available: Crystallographic data and selected bond lengths for complexes **1**, **2**, [**6-H-6**], (**7**·CH_2Cl_2), and (**8**·$CHCl_3$), crystallographic data and selected bond lengths and angles for [(η^6-*p*-cym)Ru(*N*-2-fluoro-Ph-picolinamide)Cl]$_2$$HPF_6$ ([**10-H-10**]**PF$_6$**), X-ray structures of compounds **2** and **8**, X-ray structure of **1** and **3** showing intermolecular $\pi-\pi$ stacking and short contact interactions, X-ray structure and atom numbering scheme for [(η^6-*p*-cym)Ru(*N*-2-fluoro-Ph-picolinamide)Cl]$_2$$HPF_6$ ([**10-H-10**]**PF$_6$**), low field region of the ^{1}H NMR spectrum of **7** with 3 equiv of TRISPHAT showing the presence of two stereoisomers. Effect of temperature and of pH on a mixture of the two linkage isomers of **3**, ^{1}H NMR pH titration of **1** and **7**, IC_{50} curves for compounds **1**, **3**, **4**, and 9 in human ovarian, ovarian cisplatin-resistant, and colon cancer cells and the preparation of the ligands and spectroscopic data, ESI-MS, and CHN analysis of complexes **1**−**10**. This material is available free of charge via the Internet at http://pubs.acs.org.

References

(1) Sigel, H.; Martin, R. B. Coordinating properties of the amide bond. Stability and structure of metal ion complexes of peptides and related ligands. *Chem. Rev.* **1982**, *82*, 385–426.

(2) Angel, R. L.; Fairlie, D. P.; Jackson, W. G. Linkage isomerization of (formamide-*N*)- and (acetamide-*N*)pentaamminecobalt(III) ions in water, dimethyl sulfoxide, and sulfolane. *Inorg. Chem.* **1990**, *29*, 20–28.

(3) Fairlie, D. P.; Angus, P. M.; Fenn, M. D.; Jackson, W. G. Factors influencing the nitrogen vs oxygen bonding mode of amides bound to pentaamminecobalt(III) and the kinetics and mechanism of rearrangement. *Inorg. Chem.* **1991**, *30*, 1564–1569.

(4) Fairlie, D. P.; Woon, T. C.; Wickramasinghe, W. A.; Willis, A. C. Amide-iminol tautomerism: effect of metalation. *Inorg. Chem.* **1994**, *33*, 6425–6428.

(5) Woon, T. C.; Fairlie, D. P. Amide complexes of (diethylenetriamine)platinum(II). *Inorg. Chem.* **1992**, *31*, 4069–4074.

(6) Woon, T. C.; Wickramasinghe, W. A.; Fairlie, D. P. Oxygen versus nitrogen coordination of a urea to (diethylenetriamine)platinum(II). *Inorg. Chem.* **1993**, *32*, 2190–2194.

(7) Ilan, Y.; Kapon, M. Crystal structures of (glycinamido)- and (glycinato)tetraammineruthenium(III) chelates. Effects of the metal center electronic configuration on coordinated amido and carboxylato groups. *Inorg. Chem.* **1986**, *25*, 2350–2354.

(8) Ilan, Y.; Taube, H. Isomeric forms of the complexes of tetraammineruthenium(III) and (II) with glycinamide and derivatives. *Inorg. Chem.* **1983**, *22*, 1655–1664.

(9) Chou, M. H.; Szalda, D. J.; Creutz, C.; Sutin, N. Reactivity and coordination chemistry of aromatic carboxamide $RC(O)NH_2$ and carboxylate ligands: properties of pentaammine ruthenium(II) and -(III) complexes. *Inorg. Chem.* **1994**, *33*, 1674–1684.

(10) Ford, P. C.; Rudd, D. P.; Gaunder, R.; Taube, H. Synthesis and properties of pentaamminepyridineruthenium(II) and related pentaammineruthenium complexes of aromatic nitrogen heterocycles. *J. Am. Chem. Soc.* **1968**, *90*, 1187–1194.

(11) Singh, A. K.; Balamurugan, V.; Mukherjee, R. Synthesis and characterization of low-spin and cation radical complexes of ruthenium(III) of a tridentate pyridine bis-amide ligand. *Inorg. Chem.* **2003**, *42*, 6497–6502.

(12) Jacob, W.; Mukherjee, R. Synthesis, structure, and properties of monomeric Fe(II), Co(II), and Ni(II) complexes of neutral *N*-(aryl)-2-pyridinecarboxamides. *Inorg. Chim. Acta* **2006**, *359*, 4565–4573.

(13) Patra, A. K.; Mukherjee, R. Bivalent, trivalent, and tetravalent nickel complexes with a common tridentate deprotonated pyridine bis-amide ligand. molecular structures of nickel(II) and nickel(IV) and redox activity. *Inorg. Chem.* **1999**, *38*, 1388–1393.

(14) Canty, A. J.; Lee, C. V. Relative σ donor ability of pyridines, imidazoles, and pyrazoles. *Inorg. Chim. Acta* **1981**, *54*, L205–L206.

(15) Das, A.; Peng, S.-M.; Lee, G.-H.; Bhattacharya, S. Synthesis, structure and electrochemical properties of a group of rutheniun-(III) complexes of *N*-(aryl)picolinamide. *New J. Chem.* **2004**, *28*, 712–717.

(16) Bratsos, I.; Jedner, S.; Gianferrara, T.; Alessio, E. Ruthenium anticancer compounds: challenges and expectations. *Chimia* **2007**, *61*, 692–697.

(17) Clarke, M. J.; Zhu, F. C.; Frasca, D. R. Non-platinum chemotherapeutic metallopharmaceuticals. *Chem. Rev.* **1999**, *99*, 2511–2533.

(18) Melchart, M.; Sadler, P. J. Ruthenium arene anticancer complexes. *In* Bioorganometallics, G. Jaouen, Ed.,Wiley-VCH: Weinheim 2006, pp 39–64.

(19) Peacock, A. F. A.; Sadler, P. J. Medicinal organometallic chemistry: designing metal arene complexes as anticancer agents. *Chem. Asian J.* **2008**, *3*, 1890–1899.

(20) van Rijt, S. H.; Peacock, A. F. A.; Johnstone, R. D. L.; Parsons, S.; Sadler, P. J. Organometallic osmium(II) arene anticancer complexes containing picolinate derivatives. *Inorg. Chem.* **2009**, *48*, 1753–1762.

(21) Lee, S. A.; Eyeson, R.; Cheever, M. L.; Geng, J. M.; Verkhusha, V. V.; Burd, C.; Overduin, M.; Kutateladze, T. G. Targeting of the FYVE domain to endosomal membranes is regulated by a histidine switch. *Proc. Natl. Acad. Sci. U.S.A.* **2005**, *102*, 13052–13057.

(22) Sigel, R. K. O.; Sabat, M.; Freisinger, E.; Mower, A.; Lippert, B. Metal-modified base pairs involving different donor sites of purine nucleobases: *trans*-[a(2)Pt(7,9-DimeG-*N*1)(9-EtGH-*N*7)](2+) and *trans*-[a(2)Pt(7,9-DimeG-*N*1)(9-EtG-*N*7)](+) (*a* = NH_3 or CH_3-NH_2; 9-EtGH = 9-ethylguanine; 7,9-DimeG = 7,9-dimethylguanine). Possible relevance to metalated DNA triplex structures. *Inorg. Chem.* **1999**, *38*, 1481–1490.

(23) Peacock, A. F. A.; Melchart, M.; Deeth, R. J.; Habtemariam, A.; Parsons, S.; Sadler, P. J. Osmium(II) and ruthenium(II) arene maltolato complexes: Rapid hydrolysis and nucleobase binding. *Chem.—Eur. J.* **2007**, *13*, 2601–2613.

(24) Couchman, S. M.; Jeffery, J. C.; Ward, M. D. Synthesis and coordination chemistry of the tetradentate ligands 6,6′-bis-(3-pyrazolyl)-2,2′-bipyridine and 6,6′-bis(2-hydroxyphenyl)-2,2′-bipyridine: intramolecular hydrogen-bonding in complexes of Cu(II), and a dinuclear double helicate with Ag(I). *Polyhedron* **1999**, *18*, 2633–2640.

(25) Peacock, A. F. A.; Habtemariam, A.; Fernandez, R.; Walland, V.; Fabbiani, F. P. A.; Parsons, S.; Aird, R. E.; Jodrell, D. I.; Sadler, P. J. Tuning the reactivity of osmium(II) and ruthenium(II) arene complexes under physiological conditions. *J. Am. Chem. Soc.* **2006**, *128*, 1739–1748.

(26) Peacock, A. F. A.; Habtemariam, A.; Moggach, S. A.; Prescimone, A.; Parsons, S.; Sadler, P. J. Chloro half-sandwich osmium(II) complexes: influence of chelated *N*,*N*-ligands on hydrolysis, guanine binding, and cytotoxicity. *Inorg. Chem.* **2007**, *46*, 4049–4059.

(27) Chen, H.; Parkinson, J. A.; Parsons, S.; Coxall, R. A.; Gould, R. O.; Sadler, P. J. Organometallic ruthenium(II) diamine anticancer complexes: arene-nucleobase stacking and stereospecific hydrogen-bonding in guanine adducts. *J. Am. Chem. Soc.* **2002**, *124*, 3064–3082.

(28) Liu, H. K.; Wang, F. Y.; Parkinson, J. A.; Bella, J.; Sadler, P. J. Ruthenation of duplex and single-stranded d(CGGCCG) by organometallic anticancer complexes. *Chem.—Eur. J.* **2006**, *12*, 6151–6165.

(29) Novakova, O.; Kasparkova, J.; Bursova, V.; Hofr, C.; Vojtiskova, M.; Chen, H.; Sadler, P. J.; Brabec, V. Conformation of DNA modified by monofunctional Ru(II) arene complexes: recognition by DNA binding proteins and repair. relationship to cytotoxicity. *Chem. Biol.* **2005**, *12*, 121–129.

(30) Zhang, C. X.; Lippard, S. J. New metal complexes as potential therapeutics. *Curr. Opin. Chem. Biol.* **2003**, *7*, 481–489.

(31) Brabec, V.; Novakova, O. DNA binding mode of ruthenium complexes and relationship to tumor cell toxicity. *Drug Resist. Updates* **2006**, *9*, 111–122.

(32) Jung, Y.; Lippard, S. J. Direct Cellular Responses to Platinum-Induced DNA Damage. *Chem. Rev.* **2007**, *107*, 1387–1407.

(33) Stahl, S.; Werner, H. A new family of (arene)osmium(0) and (arene)osmium(II) complexes. *Organometallics* **1990**, *9*, 1876–1881.

(34) Morris, R. E.; Aird, R. E.; Murdoch, P. D.; Chen, H. M.; Cummings, J.; Hughes, N. D.; Parsons, S.; Parkin, A.; Boyd, G.; Jodrell, D. I.; Sadler, P. J. Inhibition of cancer cell growth by ruthenium(II) arene complexes. *J. Med. Chem.* **2001**, *44*, 3616–3621.

(35) Fernandez, R.; Melchart, M.; Habtemariam, A.; Parsons, S.; Sadler, P. L. Use of chelating ligands to tune the reactive site of half-sandwich ruthenium(II)−arene anticancer complexes. *Chem.—Eur. J.* **2004**, *10*, 5173–5179.

(36) Hwang, T. L.; Shaka, A. J. Water Suppression That Works—Excitation Sculpting Using Arbitrary Wave-Forms and Pulsed-Field Gradients. *J. Magn. Reson. Ser. A* **1995**, *112*, 275–279.

(37) Cosier, J.; Glazer, A. M. A nitrogen-gas-stream cryostat for general x-ray diffraction studies. *J. Appl. Crystallogr.* **1986**, *19*, 105–107.

(38) Sheldrick, G. M. *SADABS version 2006−1*, University of Gottingen, Gottingen, Germany, 2006.

(39) Sheldrick, G. M. *SHELXL-97: Program for the Refinement of Crystal Structures*; University of Gottingen: Germany. 1997.

(40) Beurskens, P. T.; Beurskens, G.; Bosman, W. P.; de Gelder, R.; Garcia-Granda; S.; Gould, R. O.; Israel, R.; Smits, J. M. M. *Crystallography Laboratory*; University of Nijmegen, Nijmegen, The Netherlands, 1996.

(41) Altomare, A.; Cascarano, G.; Giacovazzo, C.; Guagliardi, A. Early finding of preferred orientation: a new method. *J. Appl. Crystallogr.* **1994**, *27*, 1045–1050.

(42) Betteridge, P. W.; Carruthers, J. R.; Cooper, R. I.; Prout, K.; Watkin, D. J. CRYSTALS version 12: software for guided crystal structure analysis. *J. Appl. Crystallogr.* **2003**, *36*, 1487.

(43) Otwinowski Z.; W., M. In *DENZO and SCALEPACK Programs*; Yale University: New Haven, CT. 1995.

(44) Sheldrick, G. M. *Program for the Solution of Crystal Structures*; University of Gottingen: Gottingen, Germany 1985.

(45) Altomare, A.; Burla, M. C.; Camalli, M.; Cascarano, G. L.; Giacovazzo, C.; Guagliardi, A.; Moliterni, A. G. G.; Polidori, G.; Spagna, R. SIR97: a new tool for crystal structure determination and refinement. *J. Appl. Crystallogr.* **1999**, *32*, 115–119.

(46) POVray: Persistence of Vision Raytracer.6. In *POVray: Persistence of Vision Raytracer*, 2004.

(47) Barbour, L. J. X-Seed—A software tool for supramolecular crystallography. *J. Supramol. Chem.* **2001**, *1*, 189–191.

(48) Krezel, A.; Bal, W. A formula for correlating p*K*(a) values determined in D_2O and H_2O. *J. Inorg. Biochem.* **2004**, *98*, 161–166.

(49) Skehan, P.; Storeng, R.; Scudiero, D.; Monks, A.; McMahon, J.; Vistica, D.; Warren, J. T.; Bokesch, H.; Kenney, S.; Boyd, M. R. New colorimetric cytotoxicity assay for anticancer-drug-screening. *J. Natl. Cancer Inst.* **1990**, *82*, 1107–1112.

(50) Te Velde, G.; Bickelhaupt, F. M.; Baerends, E. J.; Fonseca Guerra, C.; Van Gisbergen, S. J. A.; Snijders, J. G.; Ziegler, T. Chemistry with ADF. *J. Comput. Chem.* **2001**, *22*, 931–967.
(51) van Lenthe, E.; Baerends, E. J.; Snijders, J. G. Relativistic regular two-component Hamiltonians. *J. Chem. Phys.* **1993**, *99*, 4597–610.
(52) van Lenthe, E.; Baerends, E. J.; Snijders, J. G. Relativistic total energy using regular approximations. *J. Chem. Phys.* **1994**, *101*, 9783–9792.
(53) van Lenthe, E.; Baerends, E. J.; Snijders, J. G. Construction of the Foldy−Wouthuysen transformation and solution of the Dirac equation using large components only. *J. Chem. Phys.* **1996**, *105*, 2373–2377.
(54) van Lenthe, E.; Ehlers, A.; Baerends, E.-J. Geometry optimizations in the zero order regular approximation for relativistic effects. *J. Chem. Phys.* **1999**, *110*, 8943–8953.
(55) Van Lenthe, E.; Van Leeuwen, R.; Baerends, E. J.; Snijders, J. G. Relativistic regular two-component Hamiltonians. *Int. J. Quantum Chem.* **1996**, *57*, 281–293.
(56) Baerends, E. J.; Ellis, D. E.; Ros, P. Theoretical study of the interaction of ethylene with transition metal complexes. *Theor. Chim. Acta* **1972**, *27*, 339–354.